Received: 8 February 2023 | Revised: 26 May 2023 | Accepted: 15 June 2023

DOI: 10.1002/pro.4707

ARTICLE

THE PROTEIN SOCIETY WILEY

Convergent behavior of extended stalk regions from staphylococcal surface proteins with widely divergent sequence patterns

Alexander E. Yarawsky[1] | **Andrea L. Ori**[1,2] | **Lance R. English**[3] | **Steven T. Whitten**[3] | **Andrew B. Herr**[1,4,5]

[1]Division of Immunobiology, Cincinnati Children's Hospital Medical Center, Cincinnati, Ohio, USA

[2]Medical Sciences Baccalaureate Program, University of Cincinnati, Cincinnati, Ohio, USA

[3]Department of Chemistry and Biochemistry, Texas State University, San Marcos, Texas, USA

[4]Division of Infectious Diseases, Cincinnati Children's Hospital Medical Center, Cincinnati, Ohio, USA

[5]Department of Pediatrics, University of Cincinnati College of Medicine, Cincinnati, Ohio, USA

Correspondence
Andrew B. Herr, Division of Immunobiology, Cincinnati Children's Hospital Medical Center, 3333 Burnet Avenue, Cincinnati, OH 45229, USA.
Email: andrew.herr@cchmc.org

Present addresses
Alexander E. Yarawsky, BioAnalysis, LLC, Philadelphia, Pennsylvania, USA; Andrea L. Ori, Graduate Program in Molecular Biophysics, Johns Hopkins University, Baltimore, Maryland, USA; and Lance R. English, Department of Physical Sciences, Temple College, Temple, Texas, USA.

Funding information
National Institute of General Medical Sciences; University of Cincinnati

Review Editor: Aitziber L. Cortajarena

Abstract

Staphylococcus epidermidis and *Staphylococcus aureus* are highly problematic bacteria in hospital settings. A major challenge is their ability to form biofilms on abiotic or biotic surfaces. Biofilms are well-organized, multicellular bacterial aggregates that resist antibiotic treatment and often lead to recurrent infections. Bacterial cell wall-anchored (CWA) proteins are important players in biofilm formation and infection. Many have putative stalk-like regions or regions of low complexity near the cell wall-anchoring motif. Recent work demonstrated the strong propensity of the stalk region of *S. epidermidis* accumulation-associated protein (Aap) to remain highly extended under solution conditions that typically induce compaction. This behavior is consistent with the expected function of a stalk-like region that is covalently attached to the cell wall peptidoglycan and projects the adhesive domains of Aap away from the cell surface. In this study, we evaluate whether the ability to resist compaction is a common theme among stalk regions from various staphylococcal CWA proteins. Circular dichroism spectroscopy was used to examine secondary structure changes as a function of temperature and cosolvents along with sedimentation velocity analytical ultracentrifugation, size-exclusion chromatography, and SAXS to characterize structural characteristics in solution. All stalk regions tested are intrinsically disordered, lacking secondary structure beyond random coil and polyproline type II helix, and they all sample highly extended conformations. Remarkably, the Ser-Asp dipeptide repeat region of SdrC exhibited nearly identical behavior in solution when compared to the Aap Pro/Gly-rich region, despite highly divergent sequence patterns, indicating conservation of function by various distinct staphylococcal CWA protein stalk regions.

KEYWORDS

analytical ultracentrifugation, cell wall-anchored protein, circular dichroism, intrinsically disordered protein, size-exclusion chromatography, small-angle X-ray scattering, *Staphylococcus aureus*, *Staphylococcus epidermidis*

1 | INTRODUCTION

The gram-positive bacteria *S. aureus* and *S. epidermidis* are of major concern to the healthcare system. Hospital-acquired infections can lead to bacteremia, endocarditis, and prosthetic joint infection. Biofilm formation is a critical virulence factor, which makes these infections difficult to treat (Cardo et al., 2004; Otto, 2009; Rohde et al., 2007; Tong et al., 2015). It is well understood now that cell wall-anchored (CWA) proteins, rather than just polysaccharide intercellular adhesin, are extremely important in various stages of biofilm formation and infection (Otto, 2009; Rohde et al., 2007; Schaeffer et al., 2015; Speziale et al., 2014).

Much work has focused on the role of the structurally ordered, functional regions of various CWA proteins in biofilm formation (Speziale et al., 2014), however, the regions of low complexity—characterized by often-repetitive sequences with a limited subset of amino acids (Ntountoumi et al., 2019)—or putative stalk-like regions of these proteins are often neglected. We recently investigated the proline/glycine-rich (stalk-like) region (PGR) of the accumulation-associated protein (Aap), from *S. epidermidis*, and we found this region is intrinsically disordered, but has an unusual ability to remain extended under harsh conditions. Given the placement of this region adjacent to the cell wall, we hypothesize the ability to maintain an extended conformation could help facilitate bacterial surface attachment and intercellular accumulation of staphylococcal cells in a nascent biofilm via the functional adhesive regions of Aap (i.e., the lectin domain and B-repeat superdomain) (Yarawsky et al., 2017).

In the current study, we sought to understand if such a property was common among similar regions of low complexity from various CWA proteins (Figure 1). In addition to the stalk-like PGR region that extends from the bacterial cell wall, Aap features a putatively disordered region at the N-terminus comprised of 11 short A-repeats (Arpts) of ~16 residues each; this region is included in this study as a control intrinsically disordered polypeptide (IDP) that does not act as a stalk, given that it is not located proximal to the cell wall attachment point (Conrady et al., 2008; Hussain et al., 1997; Schaeffer et al., 2015). The N-terminal "A-domain" of Aap, including the A-repeat region and the downstream lectin domain, is important for surface adherence and adhesion to host cell ligands (Maciag et al., 2023; Macintosh et al., 2009; Roy et al., 2021). The N-terminus must be removed via SepA or other proteases for Aap-dependent biofilm accumulation to occur via Zn^{2+}-dependent assembly of the B-repeat superdomain (Paharik et al., 2016; Rohde et al., 2005). While the specific role of the A-repeat region is unclear, it may sterically inhibit or modulate intercellular adhesion via the B-repeat superdomain under resting conditions.

Also included in this study is the stalk region equivalent to the PGR of Aap found in the *S. aureus* ortholog, SasG (Corrigan et al., 2007). We hypothesize that SasG-PGR will share very similar properties as Aap-PGR, as both Aap and SasG PGRs contain a proline in every third position (Figure 1) and both adhesins adopt similar roles in biofilm formation. In both proteins, a highly extended stalk would likely facilitate the biological functions of host cell interaction as well as intercellular adhesion in the nascent biofilm after cleavage of the A-domain.

SdrC belongs to the serine-aspartate family of proteins expressed by *S. epidermidis* and *S. aureus* (McCrea et al., 2000; Speziale et al., 2014). Like Aap and SasG, these proteins are CWA and play important roles in biofilm formation, including primary attachment to host tissue through receptor binding and bacterial accumulation via homophilic interaction (McCrea et al., 2000; Speziale et al., 2014). The common scheme of serine-aspartate (Sdr) proteins is a large A-region which contains multiple IgG-like repeats involved in ligand binding or homophilic interaction, followed by several B-repeats (unrelated to the B-repeats of Aap and SasG) of ~110 residues that are elongated in structure and are capable of binding ligands such as collagen (Arrecubieta et al., 2007; Josefsson et al., 1998). Downstream of the B-repeats is the serine-aspartate repeat region, which contains a large but varying number of SD dipeptide repeats, from 56 residues in SdrG to 558 in SdrF (McCrea et al., 2000). The C-terminus of the precursor protein contains an LPXTG cell wall-anchoring motif and a hydrophobic membrane-spanning region; as with Aap and SasG, the LPXTG motif is cleaved by sortase A between the T and G residues and the threonine is covalently attached to peptidoglycan in the cell wall (McCrea et al., 2000). We hypothesize that the SD repeats of SdrC and other Sdr family members will show similar features to the PGR of Aap and SasG, in that they may be highly extended in order to traverse the peptidoglycan layers and to allow the A and B regions to extend outward for efficient binding to host tissues or accumulation via homophilic interactions. Interestingly, the SD repeats lack the high proline content we hypothesized to be important for the extended configuration of Aap-PGR to resist compaction, but they may instead rely on charge-based contributions that are lacking in Aap-PGR.

We utilized several sequence-based predictions that indicated each construct is likely to be disordered, primarily due to the lack of hydrophobic (order-promoting) residues, but in the case of the SD repeats, there is also a strong contribution from high net charge. Predictions

AaP-PGR:
AEPGKP AEPGKP AEPGKP AEPGTP AEPGKP AEPGTP AEPGKP AEPGKP AEPGKP
AEPGKP AEPGTP AEPGTP AEPGKP AEPGTP AEPGKP AEPGTP AEPGKP AESGKP
VEPGTP AQSGAP EQPNRSMHSTDNKNQ

SasG-PGR:
PKDP KGPENP EKPSRP THPSGP VNPNNP GLSKDR AKPNGP
VHSMDKNDKVKKSKIAKESVANQEKKRAE

Arpts:
N NEAPQMSSTLQAEEGS NAEAPQSEPTKAEEGG NAEAAQSEPTKAEEGG
NAEAPQSEPTKAEEGG NAEAAQSEPTKTEEGS NVKAAQSEPTKAEEGS
NAEAPQSEPTKTEEGS NAKAAQSEPTKAEEGG NAEAAQSEPTKTEEGS
NAEAPQSEPTKAEEGG NAEAPQSEPTKTEEGG NAEAPNVPTIKA

SdrC-SD:
SDSDSDSDSDSDSDSDSDSDSDSDSDSDSDNDSDSDSDSDSD AGKHTPAKPMSTVKDQHKTAKA

SD-30mer:
SDSDSDSDSDSDSDSDSDSDSDSDSDSDSD

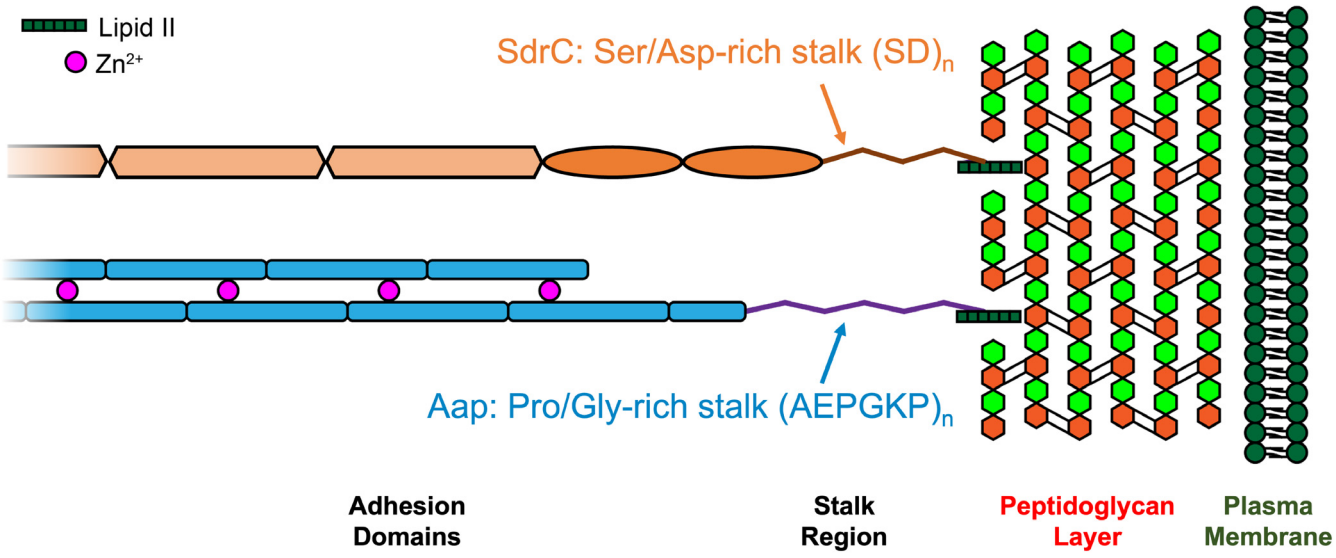

FIGURE 1 Sequences of IDP constructs. Prolines are in bold font, negatively charged residues are colored red, and positively charged residues are colored blue. Sequence repeats are separated by spaces to highlight the pattern. The illustration at the bottom highlights the location of the stalk regions relative to the peptidoglycan layer.

based on charge patterning and polyproline type II helix (PPII) propensity suggest highly extended conformations may be preferred by these sequences. Indeed, sedimentation velocity analytical ultracentrifugation (AUC) indicated high frictional ratios representative of highly extended or elongated species, which was confirmed with size-exclusion chromatography (SEC) and small-angle X-ray scattering (SAXS). A battery of experiments using circular dichroism (CD) spectroscopy revealed trends in the resistance to compaction which were proportional to predicted PPII propensity (for proline-rich sequences) or to high negative charge density (for SdrC-SD);

specifically, these sequences showed stronger resistance to perturbation by temperature or cosolvents.

2 | RESULTS

2.1 | All constructs are predicted to be disordered

Our first approach to compare these constructs was to examine sequence-based algorithms to determine their propensity to be folded (ordered) or intrinsically disordered. Uversky et al. found that the mean net charge and mean scaled hydropathy of a protein are a powerful predictor of whether or not the protein will be ordered or disordered (Uversky et al., 2000). In Figure 2a, all constructs of interest are located on the disordered side of the Uversky plot. Interestingly, while the mean scaled hydropathy values all fall within the range of 0.25–0.35, the absolute mean net charge varies much more, ranging from 0.05 to 0.50. In light of the variability in mean net charge, we sought to examine additional parameters related to charge.

Several studies have been published examining the potential effects of charge on IDP conformation. Das and Pappu have investigated the impact of charge distribution or charge mixing on IDP conformational preferences (Das & Pappu, 2013). They proposed classifying proteins based on the fraction of positively (f_+) and negatively (f_-) charged residues, resulting in the Das-Pappu plot shown in Figure 2b. Each region of this plot is discussed in detail elsewhere (Das & Pappu, 2013). Region 2 contains Aap-PGR and Aap-Arpts. This region is considered a "boundary" region of so-called Janus sequences, where the conformational ensemble may sample either globule or tadpole conformations (Region 1) or coils, hairpins, or chimeras (Region 3). SdrC-SD and SasG-PGR both just cross the boundary into Region 3, populated by strong polyampholytes. For comparison in the Das-Pappu plot, we also included an SD-30mer comprised solely of repeating SD dipeptides, which is located in Region 4 of strong negatively charged polyelectrolytes that form swollen coils (Figure 2b). The difference between SdrC-SD and the SD-30mer is the inclusion of the native C-terminal 22 residues in SdrC that deviate from the SD repeating pattern. In addition to fractional charge, the specific distribution of charged residues is an important parameter that influences the configurational properties of polypeptide chains (Das & Pappu, 2013; Sawle & Ghosh, 2015). Different parameters have been used to describe sequence charge distribution; both the κ parameter proposed by Das and Pappu (2013) and sequence charge decoration (SCD) described by Sawle and Ghosh (2015) report on the degree of charge clustering. Although they are calculated differently, a high value of κ or SCD represents highly segregated sequences (e.g., EEEEEKKKKK), which show a preference for hairpins or more compact conformations, while well-mixed sequences with low κ or SCD values (e.g., EKEKEKEKEK) experience self-avoidance due to electrostatic-repulsion and tend toward extended chains or Flory random coils (Das & Pappu, 2013; Sawle & Ghosh, 2015). The κ and SCD values for each construct are shown in Table S1, along with additional parameters relevant to charge provided by the CIDER webserver (Holehouse et al., 2017).

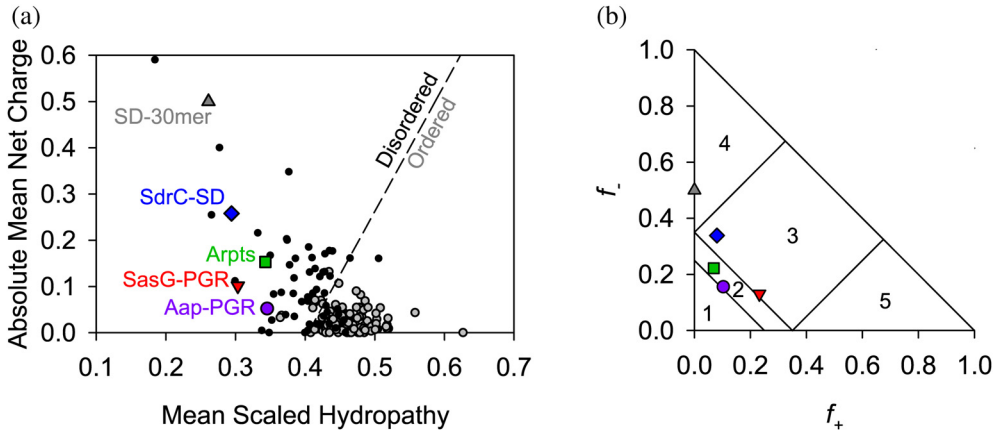

FIGURE 2 Predictions of disorder and classification of IDP constructs. The Uversky plot (a) is a powerful predictor of disorder based on net charge and hydrophathy (Uversky et al., 2000). A reference line (dashed) separates disordered proteins (black, filled circles) and ordered proteins (gray, filled circles). All IDP constructs of interest in this study fall on the "Disordered" side of the reference line. Panel (b) shows the IDPs plotted on the Das-Pappu phase plot (Das & Pappu, 2013). Symbols are consistent with (a). Numbers refer to the phase plot region (see Table S1).

A more relevant parameter in the case of Aap-PGR, SasG-PGR, and Aap-Arpts might be omega, Ω. This value considers the patterning of proline and charged residues against all other residues (Martin et al., 2016). While the implications of κ are dependent upon the fraction of charged residues (FCR), Ω is dependent on FCR and the number of proline residues. When used appropriately, such as for a sequence with mostly similarly charged residues and well-dispersed prolines, sequences with low Ω are more expanded or extended than those with high Ω (Martin et al., 2016). One should use caution when the sequence of interest contains poorly mixed charged/proline residues, as this could enable long-range electrostatic attractions leading to hairpins, or there could be steric restrictions from groups of prolines. Table S1 also lists the Ω value for each construct. For Aap-PGR, SasG-PGR, and Aap-Arpts, Ω is very low, suggesting the patterning of charged/proline residues could bias the conformational ensemble toward more extended conformations. SdrC-SD and SD-30mer contain few or no proline residues, so κ is the more appropriate parameter to consider for those constructs.

In addition to the role of charged residues described by Uversky et al. (2000) and the Pappu Lab (Das & Pappu, 2013; Mao et al., 2010; Martin et al., 2016), there are additional factors that confer conformational bias. Work from the Whitten Lab has examined the effect of polyproline type-II (PPII) helix propensity (Langridge et al., 2014; Perez et al., 2014; Tomasso et al., 2016) and α-helix propensity (English et al., 2017, 2019) on the hydrodynamic radius (R_h) of an IDP. PPII, thought to be a dominant backbone conformation in unfolded proteins (Shi et al., 2006), is a left-handed helix with three-fold rotational symmetry that is highly extended compared to an α-helix (Adzhubei et al., 2013). Tomasso et al. (2016) found the R_h values of IDPs could be predicted very well based on the PPII propensity and number of residues. Interestingly, the effect of charged residues was very weak compared to PPII propensity but could be significant where there was poor mixing of oppositely charged residues (i.e., sequences with a low κ value).

Parameters relevant to R_h prediction from PPII propensity are listed in Table S2. In the case of Aap-PGR, SasG-PGR, and Aap-Arpts, there are a high number of prolines, which could place a strong PPII-based bias on their conformations. They are also rich in other residues that have a high propensity for PPII (Elam et al., 2013; Rucker et al., 2003; Shi et al., 2005; Tomasso et al., 2016). The predicted fraction of residues in the PPII conformation, f_{PPII}, is the averaged PPII propensity (Elam et al., 2013; Tomasso et al., 2016) based on sequence composition. Aap-PGR has a higher f_{PPII} value than all other IDPs in the database used by Tomasso et al. (2016) (Table S3). SasG-PGR has the third highest f_{PPII} value, after the disordered tail of p53 (referred to as p53(1–93) Table S3) and Aap-PGR. Aap-Arpts lies at number six in the dataset of 27, while SdrC-SD and SD-30mer fall at or near the bottom of f_{PPII} values (Table S3). Also listed in Table S2 are the predicted R_h values assuming a random coil conformation that lacks strong preferences for backbone structures (R_h (coil)), predicted R_h for a random coil that samples PPII with a bias equivalent to f_{PPII} (R_h (PPII)), and predicted R_h for a random coil with a f_{PPII} bias and an additional effect owing to the net charge (R_h (PPII charge)). These values suggest which factors might influence the predicted R_h more strongly. Whether or not a protein is folded is perhaps the strongest influence on whether the global conformation is expected to be compact or expanded/extended (Langridge et al., 2014; Marsh & Forman-Kay, 2010; Perez et al., 2014; Tomasso et al., 2016; Uversky, 2002a). This R_h predictor assumes the sequence is disordered. As expected, the contribution to the predicted R_h from PPII propensity is proportional to f_{PPII}, and in the case of the IDPs with high FCR but low proline content, a contribution from the net charge can increase the predicted R_h significantly (Table S2).

2.2 | All IDPs are highly elongated monomers

Before examining the proteins by CD, we examined their global conformations by sedimentation velocity AUC and SEC. Sedimentation velocity AUC measures the rate of sedimentation (sedimentation coefficient, s) as a species moves through solution (Cantor & Schimmel, 1980; Laue & Stafford 3rd., 1999). The calculated sedimentation coefficient (s) is dependent on the size (buoyant molar mass) and shape of the species. A protein that is highly expanded or elongated will sediment more slowly, due to increased frictional resistance, than a compact protein of the same molar mass. The frictional coefficient is reported as the frictional ratio (f/f_0), where the observed frictional coefficient is divided by the frictional coefficient of a sphere of the same volume (Brown & Schuck, 2006). We performed sedimentation velocity AUC on each of the IDPs of interest (for ease of comparison, previously published data for Aap-PGR (Yarawsky et al., 2017) are included where appropriate alongside new data for SasG-PGR, Aap-Arpts, and SdrC-SD). The model-independent time-derivative analysis ($-dc/dt$; Figure 3a) was performed for the datasets, with each distribution able to be fit with a single species of molar mass similar to the sequence-based monomer mass (Table 1). The c(s) distributions (Figure 3b) reveal a single boundary. As with the dc/dt analysis, the c(s) analysis yielded estimated molar

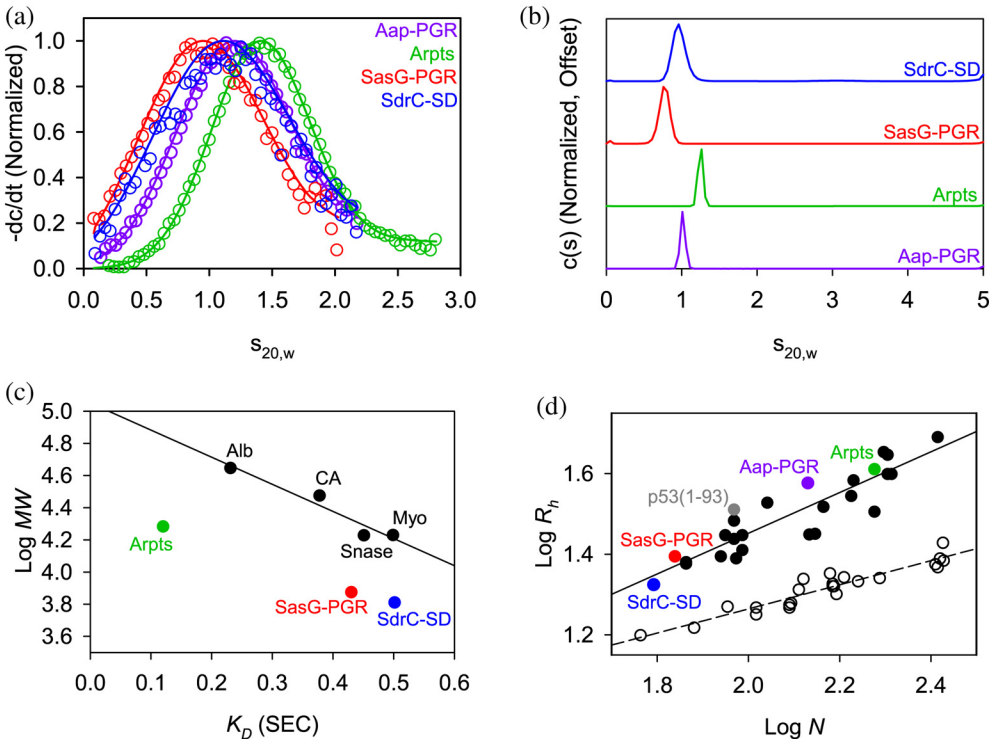

FIGURE 3 AUC and SEC indicate each construct is highly elongated and monomeric. (a) Time-derivative distributions from sedimentation velocity data. Empty markers indicate data, with every eighth data point shown for clarity. Solid lines represent the fit to a single-species model. **(**b) Sedimentation velocity AUC data suggest each construct is monomeric and highly elongated, as indicated by the fitted parameters listed in Table 1. (c) Linear relationship between SEC-measured K_D and logMW for the folded protein standards (Alb, albumin; CA, carbonic anhydrase; Myo, myoglobin; Snase, staphylococcal nuclease), showing that the IDP constructs all deviate from the trend. Aap-PGR is omitted from this plot, as it was previously analyzed using different column resin. (d) Linear relationship between log N (number of residues) and logR_h. Folded proteins (Langridge et al., 2014; Marsh & Forman-Kay, 2010) (open circles, dashed linear regression) and IDPs (Tomasso et al., 2016) (filled circles, solid linear regression) show distinct trends. SasG-PGR, Aap-Arpts, and SdrC-SD follow the trend with other IDPs. Aap-PGR data were replotted from a previous publication for ease of comparison (Yarawsky et al., 2017).

TABLE 1 Sedimentation velocity AUC parameters.

IDP	M_{seq} (kDa)	$s_{20,w}$ *(dc/dt)*	M_{exp} (kDa) *(dc/dt)*	$s_{20,w}$ (c(*s*))	f/f_0 (c(*s*))	M_{exp} (kDa) (c(*s*))	R_s (Å)	R_h (Å) (SEC)	R_h (PPII charge)
Aap-PGR	13.1	1.02	14.3	1.06	2.12	14.4	33.9	37.1	37.84
SasG-PGR	7.5	0.76	8.9	0.80	2.03	9.3	28.1	24.8	24.43
Aap-Arpts	19.1	1.25	25.6	1.30	2.52	22.2	46.2	40.8	44.06
SdrC-SD	6.4	0.91	8.4	0.97	1.93	8.1	24.7	21.1	22.15

Note: Data were analyzed using the $-dc/dt$ fitting in DCDT+ and by SEDFIT's continuous c(*s*) distribution model (Brown & Schuck, 2006) and are presented in Figure 3. The Stokes-Einstein radius, R_s, is from SEDFIT, R_h was determined experimentally by SEC, and the predicted hydrodynamic radius, R_h (PPII charge), is from Table S2, shown here for comparison.

masses similar to monomer (see Table 1). In addition to determining the molar mass, the frictional ratio (f/f_0) was also calculated and is listed in Table 1. In all cases, a very high f/f_0 is observed, indicative of highly elongated global conformations. A slight overestimate of the molar mass was observed in all cases. This is likely due to the presence of hydrodynamic nonideality, which is expected to exist to some degree for such highly elongated proteins, despite the loading concentrations being at or below 1 mg/mL (Creeth & Knight, 1965; Yarawsky et al., 2022).

In parallel to the AUC analysis, the hydrodynamic radius (R_h) of each construct was determined experimentally by SEC as previously described (Langridge et al., 2014; Yarawsky et al., 2017). Each protein was run over a G-100 Sephadex column along with a panel of well-characterized globular control proteins that were

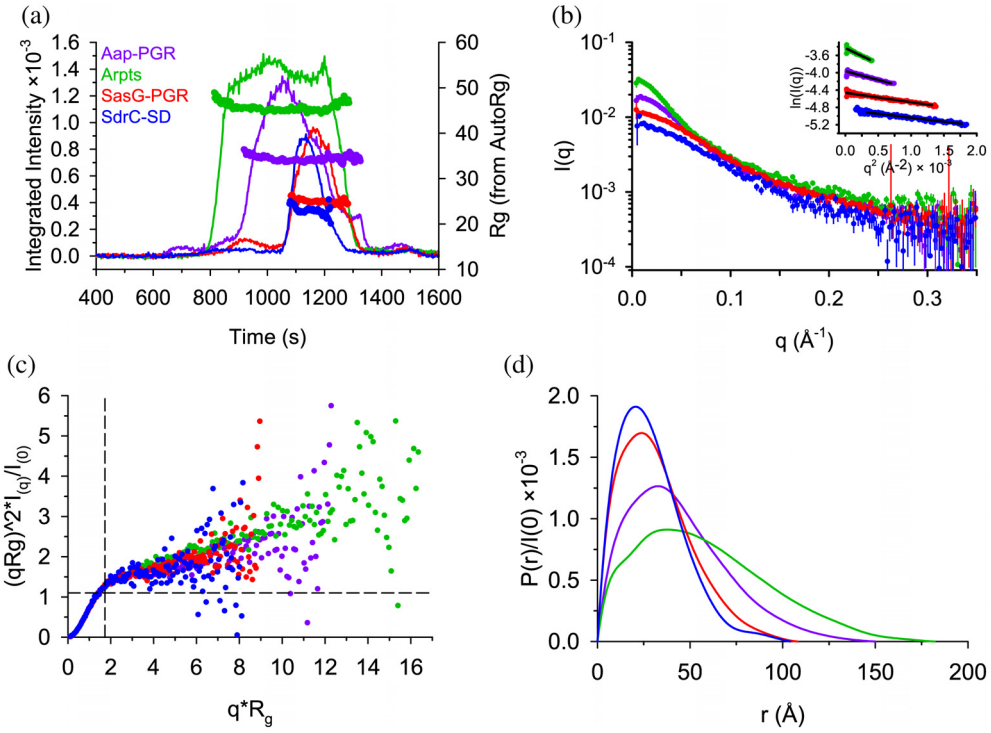

FIGURE 4 SAXS data confirm highly extended conformations for all constructs. (a) SEC-SAXS elution profiles showing scattering intensity (after buffer subtraction) and R_g calculated using AutoRg (markers). (b) The scattering profiles for each dataset, following the same color scheme as (A). The inset shows the Guinier range with lines representing the Guinier fit. (c) The normalized Kratky plot. A spherical particle should exhibit a Gaussian shaped distribution with a maximum at the intersection of the dashed lines. (d) The *P(r)* distributions normalized by *I(0)*. The D_{max} is the maximum radius in the distribution.

TABLE 2 SEC-SAXS analysis results.

IDP	R_g (Å) (Guinier)	R_g (Å) (P(r))	D_{max} (Å) (P(r))	R_h (Å) (SEC)	ρ (R_g/R_h)
Aap-PGR	35.0 ± 0.3	36.4 ± 0.2	150	37.1	0.98
SasG-PGR	25.5 ± 0.2	26.6 ± 0.1	108	24.8	1.07
Aap-Arpts	46.6 ± 0.5	47.8 ± 0.2	182	40.8	1.17
SdrC-SD	23.4 ± 0.4	24.2 ± 0.4	104	21.1	1.15

used to determine the linear relationship between the thermodynamic retention factor (K_D) and R_h. We previously determined the R_h for Aap-PGR to be 37.06 Å, which was unusually high for a low MW protein of 13.1 kDa (Yarawsky et al., 2017). Similarly, the experimental R_h determination for SasG-PGR, Aap-Arpts, and SdrC-SD yielded relatively large values of 24.8, 40.8, and 21.1 Å, respectively (Figure 3c and Table 1). As with Aap-PGR, we observed that SasG-PGR, Aap-Arpts, and SdrC-SD cluster with other disordered proteins on a plot of logR_h versus log$N$ (Figure 3d).

SEC-SAXS was used to additionally characterize the global conformation of the IDPs (Figure 4). The Guinier region of each dataset was linear and could be fitted to obtain an estimate of the radius of gyration (R_g), as shown in Figure 4b and Table 2. The Kratky Plot (Figure 4c) indicates extended particle shape due to the upward trend in the data as qR_g increases. The Kratky indications are confirmed by the P(r) distributions shown in Figure 4d, which indicate elongated shape by the tailing of the distribution, in contrast to the Gaussian shape expected for a spherical particle. Using the ratio, ρ, of the SAXS-measured R_g and SEC-measured hydrodynamic radius (R_h), another estimate of the shape can be obtained. A globular protein is expected to yield a ρ of ~0.7, while higher values indicate elongation (Burchard, 1992; Stetefeld et al., 2016). All constructs analyzed yielded values of ρ ranging from 0.98 to 1.17, consistent with an elongated state in solution (Table 2).

2.3 | CD confirms random coils with PPII bias

After confirming the constructs of interest are monomeric and highly extended, we utilized CD to measure the secondary structure of the IDPs. Random coil exhibits a minimum near 200 nm, while PPII exhibits an even stronger minimum near 200 nm, along with a weak local maximum near 220 nm (Lopes et al., 2014). It is very useful to measure the temperature dependence of the CD spectrum to examine the transition to random coil at

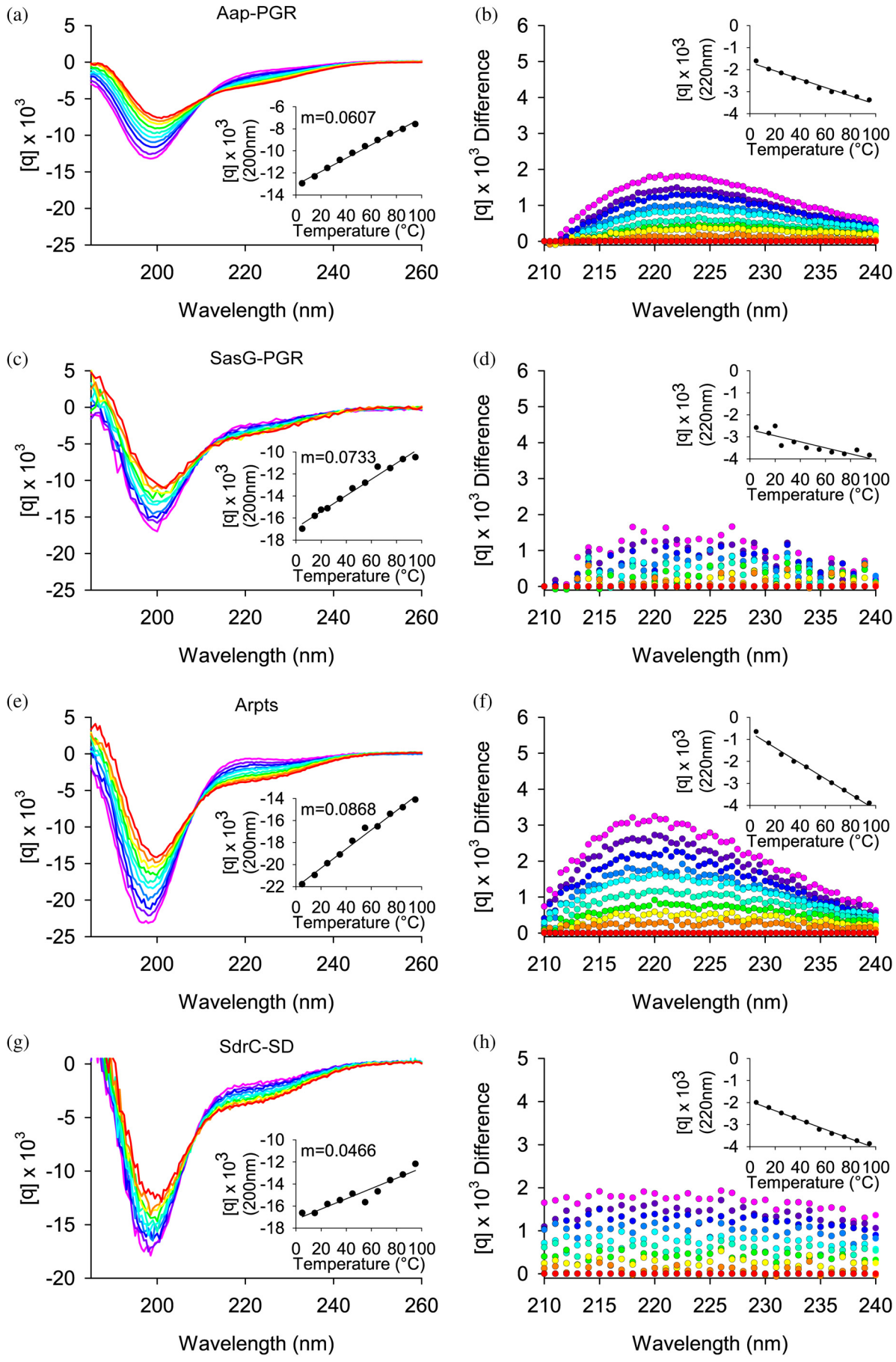

FIGURE 5 Legend on next page.

high temperatures. PPII is stabilized at low temperatures, whereas high temperatures disrupt PPII, resulting in random coil (Drake et al., 1988; Lopes et al., 2014; Perez et al., 2014; Yarawsky et al., 2017). The resulting temperature dependence is usually linear, which indicates little or no cooperativity in PPII formation (Drake et al., 1988; Schaub et al., 2012; Yarawsky et al., 2017). However, if there is significant α-helix or β-sheet content that unfolds cooperatively, one would expect to observe a sigmoidal response in the temperature dependence (Greenfield, 2004).

Figure 5 shows CD wavelength scans of Aap-PGR, SasG-PGR, SdrC-SD, and Aap-Arpts as a function of temperature. In each case, it is apparent that the primary features of the scans are the 200 nm minimum and the shift in intensity of the 220 nm signal. This strongly indicates that each IDP is composed of a mix of random coil and PPII. The insets of Figure 5a,c,e,g show the linear trend of the CD signal at the 200 nm minimum. For Aap-PGR, SasG-PGR, and Aap-Arpts, the slope (m) of the linear regression of these data trends inversely with f_{PPII}, where higher PPII propensity was associated with a shallower slope.

2.4 | Cosolvents perturb secondary structure to varying degrees

In Figure 6, we examined the effect of denaturants on the CD signal. Urea and guanidinium hydrochloride (GdnHCl) destabilize the folded state of proteins via favorable interactions with the peptide backbone and hydrophobic residues (Pace et al., 2004). Generally, GdnHCl is at least twice as effective as urea at denaturing folded proteins, but differences can be expected depending on amino acid composition. Interestingly, once a protein is unfolded, these denaturants will induce PPII (Chemes et al., 2012; Schaub et al., 2012; Tiffany & Krimm, 1973; Whittington et al., 2005). Figure 6 focuses on the region around the local maximum at 220 nm. The strong absorbance of urea and GdnHCl preclude reliable measurements below this wavelength range. Aap-PGR showed only a slight increase in PPII, indicated by the lack of significant change in the CD signal at 220 nm in the presence of urea or GdnHCl. SasG-PGR, Aap-Arpts, and SdrC-SD showed larger increases around 220 nm, especially at 4°C where PPII is more stable, suggesting a larger increase in the PPII content upon urea and GdnHCl addition. As seen with the temperature dependence in Figure 5, the magnitude of the changes is (qualitatively) inversely proportional to f_{PPII} for Aap-PGR, SasG-PGR, and Aap-Arpts, but the data for SdrC-SD most closely resemble Aap-PGR despite having a low f_{PPII} and higher values of κ and SCD. A possible interpretation of these data is that Aap-PGR does not show much of an increase in PPII content, because it already has a high PPII content (high f_{PPII}), whereas Aap-Arpts has a lower inherent PPII content in its native state and thus is more susceptible to the further denaturant-induced PPII transition. Figure 7 shows similar CD measurements in the presence of a stabilizing osmolyte, TMAO, or an alcohol, TFE. TMAO is a cosolvent that is capable of inducing compact conformations (often the functional native state for folded proteins), primarily through strongly unfavorable interactions with the peptide backbone. TMAO is particularly useful, because it does not force a specific structure, it simply destabilizes the unfolded or expanded state, which results in a shift in the equilibrium from unfolded states to the folded, native state (Auton et al., 2011; Baskakov & Bolen, 1998; Bolen & Baskakov, 2001; Pace et al., 2004). This is in stark contrast to TFE, which induces α-helix formation, even when this is non-native (Baskakov et al., 1999; Buck et al., 1995; Chemes et al., 2012; Fan et al., 1993; Sonnichsen et al., 1992).

The addition of TMAO to Aap-PGR or SdrC-SD had essentially no effect (Figure 7a,d). We previously hypothesized this was due to the moderately high frequency of charged residues, which form favorable interactions with TMAO, and therefore, are seemingly able to counter the backbone-TMAO effects (Auton et al., 2011; Yarawsky et al., 2017). If this is a valid explanation for the lack of effect, then we should also see a similar result for SasG-PGR and Aap-Arpts, which have a greater FCR (Table S1). Indeed, we see a little to no effect of TMAO on the CD spectrum of these two IDPs, although some difference is observed at low temperatures in both cases (Figure 7). A lack of response to TMAO has been

FIGURE 5 Circular dichroism wavelength scans show constructs have primarily random coil and PPII helix content. (a) shows the wavelength scans for Aap-PGR from 5°C to 95°C (cool to warm colors), while (b) shows the difference of each scan minus the 95°C scan. This highlights the shift in the local maximum around 220 nm. The insets highlight the linearity of the CD signal at 200 nm (a) or 220 nm (b). Data are shown for SasG-PGR (c, d), Aap-Arpts (e, f), and SdrC-SD (g, h). The slope determined by linear regression of the CD signal (200 nm) versus temperature is listed as "m." Aap-PGR data were replotted from a previous publication for ease of comparison (Yarawsky et al., 2017).

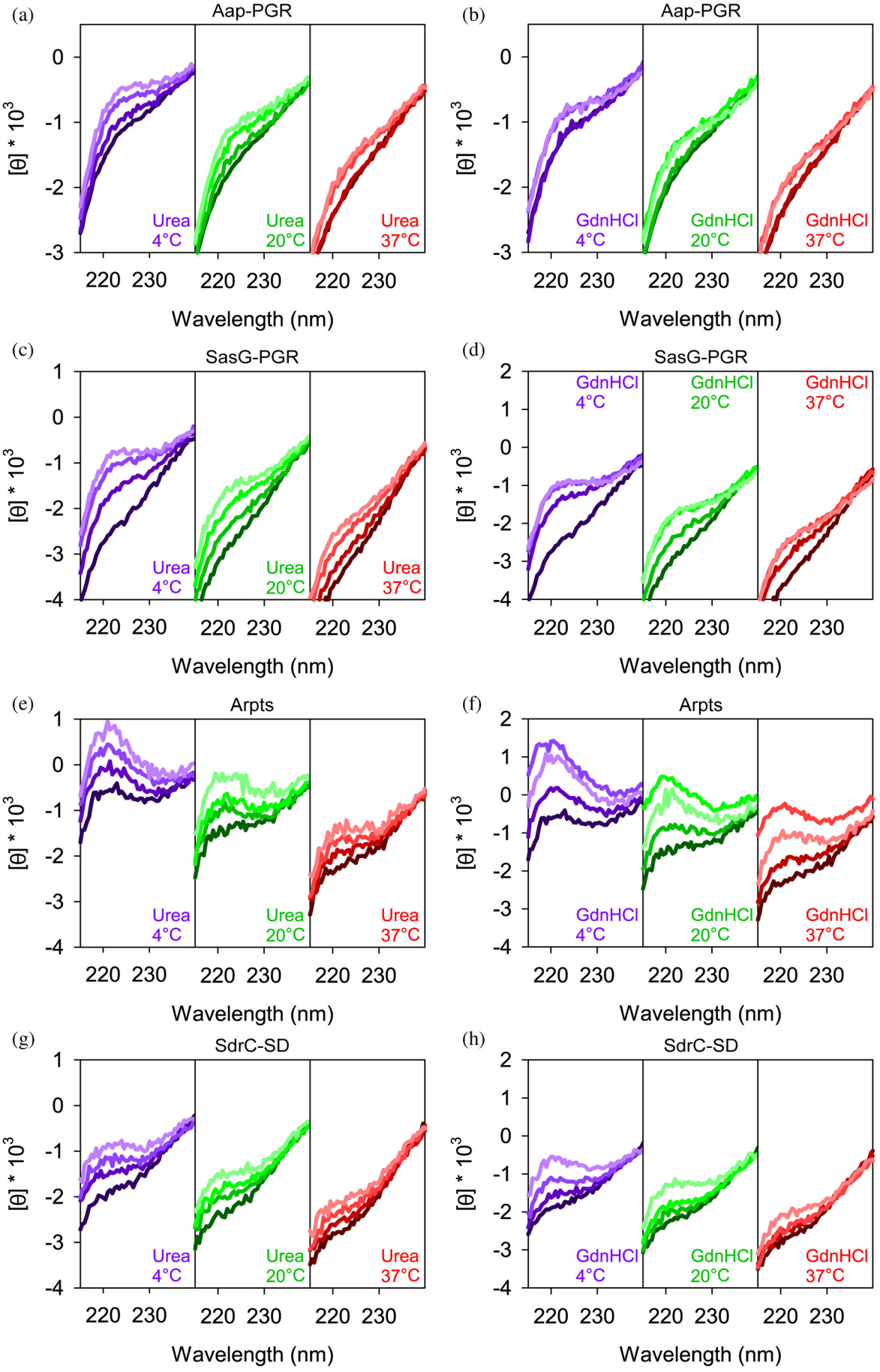

FIGURE 6 Legend on next page.

observed in other IDPs, including myelin basic protein (Hill et al., 2002) and Starmaker-like protein (Rozycka et al., 2014), which also have high FCR values of 24% and 47%. These two proteins have very low proline content (3% and 6%), so while proline also has a favorable interaction with TMAO, the charged residues are likely the most dominant factor in these cases (Auton et al., 2011). However, the decreased proline content in SasG-PGR and Aap-Arpts (Table S1) may allow for the slight effect of TMAO (Figure 7). The lack of a response to TMAO could also suggest that the native state is already populated, and there is not a separate, compact state which might be induced upon binding of a ligand as is the case with some IDPs (Uversky, 2002b; van der Lee et al., 2014).

The response to TFE was much greater than TMAO (Figure 7). As discussed elsewhere, Aap-PGR has an apparent shift from PPII to random coil upon TFE addition, but no indication of α-helix formation (Yarawsky et al., 2017). This is not surprising due to the high frequency of proline, which sterically prohibits α-helix formation. However, we expect that with the lower frequency of proline in SasG-PGR and Aap-Arpts, TFE might have a stronger effect. Indeed, we do see a much more significant effect of TFE on SasG-PGR and Aap-Arpts. CD spectra show minima at 222 nm and 208 nm, indicative of α-helix content (Greenfield, 2004). While both of these proteins show clear development of the local minimum around 222 nm and a shift of the ~200 nm minimum toward the 208 nm minimum, there are potentially interesting differences. For SasG-PGR, there is little or no weakening of the ~200–208 nm minimum, while Aap-Arpts (and Aap-PGR) show a strong weakening of this signal. Once again, the TFE response seen for SdrC-SD shows striking resemblance to that of Aap-PGR, despite the differences in f_{PPII}, f-, FCR, NCPR, and κ or SCD for the two sequences. Despite the paucity of prolines in SdrC-SD, this highly negatively charged construct showed almost a complete resistance to TFE-induced folding into α-helical secondary structures.

3 | DISCUSSION

To complement our prior investigation of Aap-PGR that forms an extended conformation and resists compaction (Yarawsky et al., 2017), we chose other low-complexity, stalk-like regions from staphylococcal adhesins to investigate and compare to Aap-PGR. These regions include the equivalent region of SasG, the *S. aureus* ortholog of Aap, and the serine-aspartate region of SdrC, which spans the space between the functional domain(s) and the cell wall-anchoring motif of this protein (McCrea et al., 2000). The Arpt region of Aap was included as a control IDP sequence that does not function as a stalk.

All constructs tested were predicted to be disordered in solution; each sequence was enriched with polar and charged (disorder-promoting) residues and was lacking in hydrophobic (order-promoting) residues (Dunker et al., 2001; Uversky, 2002b). Experimental values for the hydrodynamic radius (R_h) of each sequence closely matched predictions based on PPII propensity and charge effects, suggesting that PPII was a strong contributor to R_h in sequences with substantial proline content, although charge effects appear to be more dominant in the non-proline sequences. Sedimentation velocity AUC showed that each IDP is monomeric and exists in highly elongated conformations (Figure 3 and Table 1). The calculated radius of gyration (R_g) and Stokes-Einstein radius (R_s) trends well with both the experimentally determined R_h and the predicted R_h based on PPII and charge (Table 1).

Using CD, we verified that Aap-PGR, SasG-PGR, Aap-Arpts, and SdrC-SD exist in a PPII-random coil equilibrium, which can be modulated by temperature (Figure 4). The dependence of the CD spectra on temperature correlated with the predicted f_{PPII} for the sequences with low values of kappa (i.e., Aap-PGR, SasG-PGR, and Aap-Arpts), whereas SdrC-SD behaved like Aap-PGR despite a low predicted f_{PPII}. Likewise, the ability of chemical denaturants to increase the PPII signal showed an inverse trend with f_{PPII} for the low-kappa constructs.

With all IDPs tested, there was very little change in the CD spectra upon TMAO addition (Figure 7). This is likely due to the high FCR, with some additional contribution from proline content. It may also suggest that these IDPs do not form additional compact states, but remain disordered in their native states. This is in line with our hypothesis stating that SasG-PGR and SdrC-SD both form an extended stalk that is resistant to compaction, like Aap-PGR (Yarawsky et al., 2017). Although we have not addressed the role of molecular crowding agents on the compaction of these IDP sequences, investigations of other IDPs including α-synuclein, PCET peptide, and

FIGURE 6 Constructs respond to denaturants to different extents. Concentrations of urea were 0, 2, 4, 6 M, colored from darkest to lightest line colors. Plots show 0, 2, 4, 6 M GdnHCl using the same color scheme. Aap-PGR data were replotted from a previous publication for ease of comparison (Yarawsky et al., 2017).

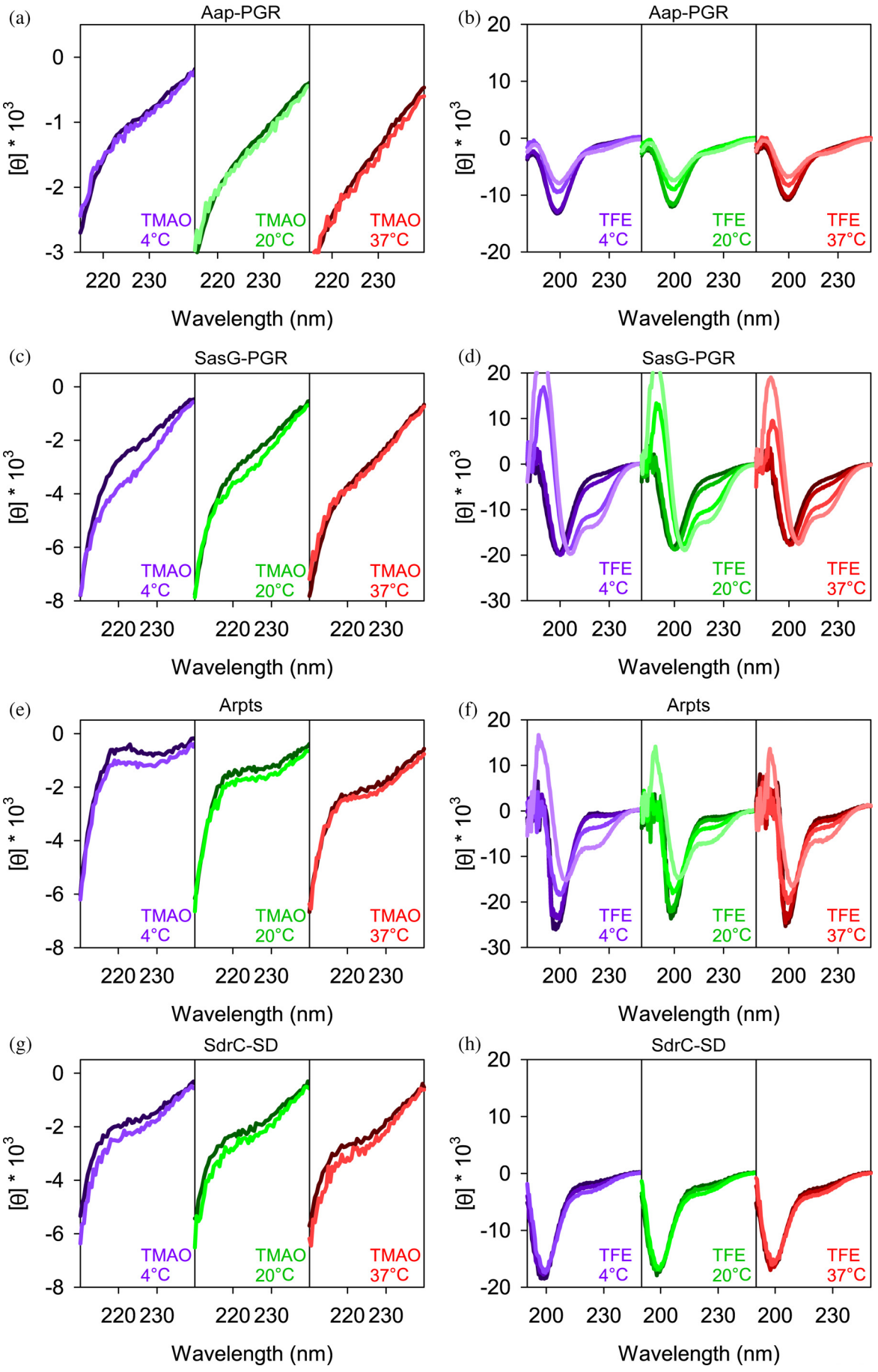

FIGURE 7 Legend on next page.

p53 CTD consistently found that TMAO or TFE had a stronger impact on compaction or induced folding of these IDPs than did molecular crowding agents (Kumar et al., 2020; McNulty et al., 2006; Munishkina et al., 2004; Sharma et al., 2020; Uversky, 2009); likewise, high concentrations of molecular crowders did not induce compaction or folding in the IDPs FosAD or p27ID (Flaugh & Lumb, 2001). These data on a variety of other IDPs suggest that molecular crowders would not be expected to induce compaction of these stalk regions to any significant degree, given their resistance to TMAO.

The addition of α-helix-inducing TFE had more significant effects than TMAO on all low-kappa IDPs. In Aap-PGR, there are prolines in every third position, disfavoring helix formation in these regions. SasG-PGR also contains a proline in every third position throughout the first half of the region, however, the second half becomes more variable and lacks proline residues. This likely allows TFE-induced α-helix formation in the latter half of the SasG-PGR sequence. While the Aap-Arpts sequence contains several prolines, they are spaced out (∼11–15 residues apart) which could allow short, interspersed α-helices to form (the average length of an α-helix is 10–15 residues (Creighton, 1993)). Notably, the Aap-Arpts sequence is distinct from the other constructs tested in that its location at the N-terminus of Aap is inconsistent with a stalk-like function; although it showed minimal change in its far-UV CD spectrum in the presence of TMAO, it was able to form a significant degree of helical content at high TFE concentrations. The role of the A-repeat region of Aap is unclear, but its TFE response indicates that Aap-Arpts could undergo induced folding, perhaps upon interaction with the lectin domain or B-repeat superdomain. SdrC-SD, like Aap-PGR, showed essentially no change upon addition of TFE, despite having very few prolines (3% of the sequence).

Remarkably, Aap-PGR and SdrC-SD, the two stalk constructs that were most divergent in sequence pattern, showed nearly identical behavior in solution. Both formed highly extended conformations by AUC and SAXS, demonstrated the least temperature dependence (based on the inset CD slopes in Figure 4), and showed minimal response to denaturants or osmolytes. In particular, both Aap-PGR and SdrC-SD were highly resistant to compaction, based on their nearly complete lack of response to TFE or TMAO. Despite these similarities in structural character, Aap-PGR and SdrC-SD occupy disparate regions of the Das-Pappu plot, with Aap-PGR falling in the boundary region of Janus sequences and SdrC-SD occupying the strong polyampholyte region. Among the sequences tested, Aap-PGR and SdrC-SD are on opposite extremes in terms of FCR, FPR, and kappa; the only similarity based on sequence parameters is Ω, since both sequences have lower values compared to SasG-PGR or Aap-Arpts. Thus, our data indicate that both high proline/PPII content (in Aap-PGR) and high electrostatic repulsion between negative residues (in SdrC-SD) result in similar self-avoiding configurations that result in highly extended, compaction-resistant stalk-like behavior.

It is very common for staphylococcal CWA proteins to feature low-complexity sequences predicted to be intrinsically disordered at the extreme C-terminus; these regions presumably function as an extended stalk. Table 3 lists a series of CWA proteins containing C-terminal LPXTG motifs from *S. aureus* or *S. epidermidis* with known or suspected adhesion functions and describes the characteristics of the low-complexity sequence regions upstream of the LPXTG sortase motifs. Of these 17 CWA proteins with adhesin-like functions, 82% have either SD-rich repeats (9 of 17) or proline-rich repeats (5 of 17) at the C-terminus that are expected to show highly elongated, compaction-resistant stalk behavior as seen for SdrC-SD and Aap-PGR. The results from this work indicate that such stalk regions share structural behavior that can be encoded by highly divergent sequence patterns such as high PPII propensity due to repeating proline residues or electrostatic repulsion due to charge effects (e.g., high values of f- or kappa). The necessity for multiple mechanisms to achieve similar stalk-like behavior might be related to environmental conditions in distinct niches (e.g., colonizing skin versus forming biofilm on heart valves or an implanted device) or to specific interactions with other macromolecules needed for particular functions. For example, the stalk region may engage with various macromolecular components comprising the biofilm matrix. A stalk with a high negative charge density (e.g., SD repeats in the Sdr family of proteins) could interact with the positively-charged biofilm polysaccharide PIA/PNAG or with zwitterionic teichoic acids in the biofilm matrix. Furthermore, context-dependent

FIGURE 7 Comparison of IDP responses to TMAO and TFE. Concentrations of TMAO (a, c, e, and g) were 0 (dark line) and 3 M (light line). The ability for TFE to perturb the secondary structure is shown in (b, d, f, and h). TFE concentrations were 0, 15%, 45%, and 75% (from dark lines to light lines) except for panel H, where 75% TFE led to aggregation of SdrC-SD. Aap-PGR data were replotted from a previous publication for ease of comparison (Yarawsky et al., 2017).

TABLE 3 Stalk regions in adhesin-like staphylococcal CWA proteins.

Protein	Ligand(s)[a]	Family[b]	Length: LCR (Total)	SD repeats	Prolines	Das-Pappu region	FCR[c]	FPR	f_{PPII}[d]	NCPR	Kappa	SCD[e]	Omega
SD-rich													
SdrC	Self, β-neurexin	Clf-Sdr	170 (193)	83	2	4	0.505	0.010	0.289	−0.479	0.056	110.90	0.00195
SdrD	Desmoglein-1	Clf-Sdr	142 (165)	71	2	4	0.466	0.012	0.290	−0.415	0.107	82.04	0.00348
SdrE	Factor H	Clf-Sdr	158 (181)	79	2	4	0.467	0.011	0.288	−0.406	0.125	99.61	0.00299
SdrF (*S. epi*)	Collagen	Clf-Sdr	170 (193)	84	2	4	0.470	0.010	0.289	−0.414	0.114	113.55	0.00280
SdrG (*S. epi*)	Fibrinogen (β)	Clf-Sdr	140 (163)	69	2	4	0.472	0.012	0.293	−0.420	0.106	79.96	0.00264
Pls	Unknown	G5-E	294 (309)	112	1	4	0.466	0.003	0.286	−0.405	0.125	325.06	0.00298
ClfA	Fibrinogen (γ), Factor I	Clf-Sdr	323 (352)	130	10	4	0.423	0.028	0.289	−0.401	0.101	260.80	0.03617
ClfB	Fibrinogen (α), Cytokeratin 8, Cytokeratin 10, Loricrin	Clf-Sdr	252 (286)	99	20	4	0.451	0.070	0.337	−0.409	0.105	196.05	0.04653
SesJ (*S. epi*)	Plasminogen	Clf-Sdr	213 (217)	36	0	4	0.378	0	0.288	−0.378	0.052	121.12	0.02044
Pro-rich													
Aap (*S. epi*)	Self	G5-E	126 (138)	0	40	2	0.261	0.290	0.537	−0.043	0.058	0.40	0.03154
SasG	Self	G5-E	40 (69)	0	12	3	0.362	0.174	0.476	0.101	0.096	1.11	0.07106
CNA	Collagen, C1q	Clf-Sdr	55 (58)	0	15	3	0.431	0.259	0.554	0.052	0.071	−0.08	0.09578
FnbpA	Fibronectin, Fibrinogen (γ)	Clf-Sdr	76 (108)	0	36	2	0.269	0.333	0.596	−0.046	0.209	−1.76	0.04935
FnbpB	Fibronectin, Fibrinogen (α), Elastin	Clf-Sdr	62 (94)	0	29	2	0.277	0.309	0.584	−0.021	0.205	−1.74	0.05606
Other													
SraP (SasA)	Sialoprotein, gp340	SRRP	73 (80)	2	2	1	0.138	0.025	0.318	−0.037	0.153	−0.06	0.45721
FmtB (SasB)	Unknown	Other	57 (58)	0	1	1	0.190	0.017	0.368	0.052	0.342	−0.40	0.28539
SasC	Self	Other	177 (220)	2	9	2	0.323	0.041	0.390	−0.023	0.147	−0.06	0.12394

[a]Ligand specificities for the LPXTG proteins are according to Arrecubieta et al. (2007), Davis et al. (2001), Formosa-Dague et al. (2016), Foster (2020), Schneewind (2019), and Yang et al. (2014a).
[b]The families of CWA proteins are listed according to Foster et al. (2014), Speziale et al. (2014), and Yang et al. (2014b).
[c]Sequence parameters were calculated using the CIDER server (http://pappulab.wustl.edu/CIDER/) (Das & Pappu, 2013; Martin et al., 2016).
[d]f_{PPII} was calculated using the Tomasso et al. algorithm (Tomasso et al., 2016).
[e]SCD was calculated using the equation for SCD provided in Sawle and Ghosh (Sawle & Ghosh, 2015).

modification of particular sequences in stalk regions can also provide functional specialization; for example, glycosylation of SD repeats of ClfA, ClfB, SdrC, SdrD, and SdrE by specific glycosyltransferases confers resistance to proteolysis (Hazenbos et al., 2013) and glycosylation of the SD-rich region of Pls promotes biofilm formation (Bleiziffer et al., 2017). Approaches such as swapping stalk regions between CWA proteins among different bacteria or reducing the PPII propensity of specific stalk regions and testing the capacity for biofilm formation or host tissue adherence would provide additional insights into the biological implications of these observations.

4 | MATERIALS AND METHODS

4.1 | Cloning and protein expression

SasG-PGR, Aap-Arpts, and SdrC-SD genes were ordered as IDT gBlocks with 5' CACC sequences for cloning into the Gateway Cloning System via pENTR/D-TOPO reaction, followed by TEV cleavage sites (ENLYQF/G) and the sequences in Figure 1, followed by a stop codon. Each gene was transferred from the pENTR vector to a destination vector containing an N-terminal His_6 tag and maltose binding protein (MBP), which was kindly provided by Dr. Artem Evdokimov. Aap-PGR DNA was synthesized by LifeTechnologies GeneArt® as previously described and moved into the same His_6-MBP destination vector (Yarawsky et al., 2017). SD-30mer was ordered as a peptide from Peptide 2.0 at ≥95% purity.

BLR(DE3) cells were transformed with the destination vector containing the gene of interest. Overnight cultures were grown at 37°C, then 25 mL used to inoculate 1 L LB broth containing ampicillin and tetracycline for antibiotic selection. The cultures were grown to an OD_{600} of 0.8–1.0 at 37°C, shaking at 200–250 rpm. The cultures were then placed in an ice bath until cooled to 10°C. At this point, ethanol was added to 2% final concentration (volume/volume) and IPTG to 200 μM. The cultures were placed back into a shaker to incubate overnight at 20°C. The following morning, cultures were centrifuged at 4500 rpm for 1 h, the supernatants discarded, and the pellets resuspended in 20 mM Tris (pH 7.4) and 300–500 mM NaCl. Resuspended pellets were stored at −20°C.

4.2 | Protein purification

Frozen pellets were thawed, sonicated to lyse the bacteria, centrifuged for 45 min at 14,000 rpm, the supernatant filtered through a 0.22 μm filter, and the protein purified by Ni^{2+}-affinity chromatography using an Äkta FPLC Chromatography System (GE Healthcare). The fusion proteins were eluted with a gradient of 0–1 M imidazole and dialyzed into 20 mM Tris (pH 7.4) and 300 mM NaCl. The protein was then incubated with TEV protease for 6–8 h at room temperature in the presence of 5 mM β-mercaptoethanol. A subtractive Ni^{2+}-affinity step was performed to capture uncleaved His_6-tagged fusion protein, His_6-tagged MBP, and His_6-tagged TEV protease, while cleaved protein of interest did not interact with the Ni^{2+}-affinity column and was captured in the flow-through. The cleaved protein of interest was then purified by size exclusion chromatography (SEC) using a Superdex 75 (S75) prep grade column (GE Healthcare) with 20 mM KPO_4, 150 mM NaCl (pH 7.4) as the running buffer. For SdrC-SD and SasG-PGR, only fractions containing the highest purity of full-length protein were collected from the S75 elution, as judged by silver-stained SDS-PAGE. For Aap-PGR and SasG-PGR, after the S75 purification, a weak anion exchange column (ANX, GE Healthcare) was used to remove contaminants or degraded species using a salt gradient (20 mM KPO_4, 50 mM NaCl, pH 7.4 to 20 mM KPO_4, 1 M NaCl, pH 7.4). Aap-PGR was collected in the flow-through, while contaminants bound to the ANX column. The Arpts construct was eluted from an ANX weak anion exchange column (GE Healthcare) across the NaCl gradient described above.

4.3 | Analytical ultracentrifugation

Sedimentation velocity experiments were performed on a Beckman Coulter XL-I AUC, using 1.2 cm two-sector epon-charcoal centerpieces. Experiments were performed at 48,000 rpm at 20°C in a An-60 Ti rotor and were continued until sedimentation was complete or back-diffusion became obvious in the raw data (~20–24 h). Interference optics were used alongside absorbance near 230 nm. Concentration estimates were obtained from the interference data. The samples were examined after dialysis or size exclusion chromatography into 20 mM KPO_4, 150 mM NaCl, pH 7.4. Data analysis was completed in SEDFIT using the continuous c(s) distribution model (Brown & Schuck, 2006) and DCDT+ (Philo, 2006; Stafford, 1992) with fitting performed against the *dc/dt* distribution (Philo, 2000) using a single-species model. SEDNTERP was used to estimate partial specific volume, buffer density and viscosity, and the fringes per mg/mL at 655 nm (Laue et al., 1992).

4.4 | Circular dichroism

An Aviv 215 spectrophotometer was used to perform CD measurements. The instrument is equipped with an Aviv

peltier junction temperature control system. A 0.05 cm quartz cuvette (Hellma Analytics) was used for all measurements. Temperature-dependence experiments were performed using protein dialyzed into 20 mM potassium phosphate (pH 7.4) and 50 mM NaF. For cosolvent experiments, concentrated protein samples were mixed with appropriate amounts of cosolvent or water to match protein concentrations within experiments. Urea used was 8 M ultra-pure grade solution (Amresco), GdnHCl was 8 M high purity solution (Pierce), TFE was >99.0% purity (Sigma-Aldrich), and TMAO was 95% solid (Sigma-Aldrich) which was dissolved into water before addition to samples. All protein-cosolvent spectra were subtracted from buffer blanks which contained equal amounts of cosolvent at each temperature.

To convert data to mean residue ellipticity, $[\theta]$, Equation (1) was used. In this equation, θ is raw machine units output by the instrument, MRW is the mean residue weight, l is the path length of 0.05 cm, and c is the concentration in mg/mL units.

$$[\theta] = \frac{\theta \times MRW}{10 \times l \times c} \quad (1)$$

4.5 | Small-angle X-ray scattering

SAXS data were collected at BioCAT (beamline 18ID at the Advanced Photon Source, Chicago, Illinois, US) with in-line SEC. Samples were dialyzed into 20 mM KPO_4, 150 mM NaCl, pH 7.4. A Superdex 75 Increase 10/300 GL column (Cytiva) was used in conjunction with an Äkta Pure FPLC (GE). The flow rate was 0.6 mL/min, the elution was monitored by UV at 280 nm, and the flow path was directed through the SAXS flow cell. The flow cell consisted of a 1 mm (internal diameter) quartz capillary with ~20 μm walls. A coflowing buffer sheath separated sample from capillary walls, helping to prevent radiation damage (Kirby et al., 2016). Scattering intensity was recorded using a Pilatus3 X 1 M (Dectris) detector which was 3.6 m from the sample, yielding a q-range of 0.005–0.35 $Å^{-1}$. Exposures of 0.5 s were acquired every 1 s during elution. Data reduction was performed using BioXTAS RAW 1.6.0 (Hopkins et al., 2017). Buffer blanks were created using regions flanking the elution peaks which showed baseline scattering intensity. I(q) versus q curves were produced by subtracting buffer blanks from elution peaks and used for downstream analysis. SAXS analysis was performed using BioXTAS RAW 2.1.0 (Hopkins et al., 2017), which called various functions from ATSAS 3.0.3 (Konarev et al., 2003; Manalastas-Cantos et al., 2021).

4.6 | Size-exclusion chromatography

Sephadex G-100 (GE Healthcare) was equilibrated in 10 mM sodium phosphate (pH 7.0) and 100 mM NaCl. A Bio-Rad BioLogic LP System was used to monitor UV absorbance at 280 nm to determine elution volumes (V_e). Concentrated samples of SasG-PGR, Aap-Arpts, and SdrC-SD at 2–3 mg/mL and at a volume of 80 μL were measured by SEC, as previously described for Aap-PGR (Yarawsky et al., 2017). To determine the void (V_0) and total column volume (V_t), we ran 10 μL of 3 mg/mL blue dextran and 0.03 mg/mL 2,4-dinitrophenyl-L-aspartate through the column separately from the proteins. The thermodynamic retention factor K_D was calculated using Equation (2):

$$K_D = (V_e - V_0)/(V_t - V_0). \quad (2)$$

To determine the hydrodynamic radius of SasG-PGR, Aap-Arpts, and SdrC-SD, R_h measured previously by dynamic light scattering (DLS) for a set of globular protein standards were plotted against the experimentally determined K_D values. The protein standards were nuclease, carbonic anhydrase, myoglobin and albumin; DLS-measured R_h were 22.4, 26.8, 22.7, and 35.6 Å, respectively (English et al., 2017). These DLS-measured values compare favorably to R_h estimated from their crystal structures (English et al., 2017). A linear regression was performed on these protein standards. The K_D of SasG-PGR, Aap-Arpts, and SdrC-SD was inserted into the linear equation of best fit to determine the R_h.

4.7 | R_h prediction

The previously described algorithm utilizes information regarding the PPII propensity to predict R_h of an IDP based on the amino acid sequence (Tomasso et al., 2016). To predict the hydrodynamic radius (R_h) of a protein based on intrinsic PPII propensities, a power-law scaling relationship (Equation 3) was used which is based on the number of residues (N) and the fraction of polyproline type II helix in the peptide chain ($f_{PPII,chain}$):

$$R_{h,PPII} = 2.16 \cdot N^{0.503 - 0.11 \cdot ln\left(1 - f_{PPII,chain}\right)} \quad (3)$$

The chain propensity for PPII structure, $f_{PPII,chain}$, is based on the experimental scale from Hilser (Elam et al., 2013) that utilized a peptide host–guest system in which the *Caenorhabditis elegans* Sem-5 SH3 domain binds a peptide in the PPII conformation. A non-interacting residue of the peptide was substituted for each

amino acid before binding was measured by isothermal titration calorimetry. The value for $f_{PPII,chain}$ in Equation (3) was determined by Equation (4), where N is the number of residues and $PPII_{prop}$ is the PPII propensity from the Hilser scale for each amino acid in the sequence from 1 to N:

$$f_{PPII,chain} = \left[\sum PPII_{prop}\right]/N \quad (4)$$

The error in the predicted R_h across many IDPs was found to correlate best with the net charge (English et al., 2017). Based on this observation, we modified the original predictor to give Equation (5):

$$R_{h,PPII\ charge} = 2.16 \cdot N^{0.503-0.11\cdot ln\left(1-f_{PPII,\ chain}\right)} + 0.25 \cdot |Q_{net}| - 0.31 \cdot N^{0.5} \quad (5)$$

The net charge, Q_{net}, is calculated from sequence as the number of lysine and arginine residues minus the number of aspartic acid and glutamic acid. Predicting R_h from Equation (5) for the three proteins yields 24.4 Å for SasG-PGR, 44.1 Å for Aap-Arpts, and 22.2 Å for SdrC-SD, based on their predicted values for $f_{PPII,chain}$ and net charge (Table S2).

4.8 | Sequence analysis of staphylococcal CWA proteins

The sequences of LPXTG-containing CWA proteins with adhesin-like function from *S. aureus* and *S. epidermidis* were submitted to the PlaToLoCo server (https://platoloco.aei.polsl.pl/) to identify potential low-complexity regions (LCRs) upstream of each protein's LPXTG motif (Jarnot et al., 2020). The server produces a consensus view from several algorithms that identify LCRs, including SEG, CAST, fLPS, and SIMPLE. We used multiple algorithms to identify a consensus region upstream of the LPXTG motif in each protein; in general, CAST provided consistent predictions for the Pro-rich proteins whereas SEG performed better at yielding consistent predictions for the SD-rich proteins. Table 3 lists the number of residues in the LCR compared to the total number of residues, which includes the sequence between the end of the LCR and the beginning of the LPXTG motif. The CIDER server (http://pappulab.wustl.edu/CIDER/) (Das & Pappu, 2013; Martin et al., 2016) was used to predict Das-Pappu plot regions as well as FCR, NCPR, and omega values; f_{PPII} was calculated by the Tomasso et al. algorithm (Tomasso et al., 2016), SCD was calculated using the equation for SCD provided in Sawle & Ghosh (Sawle & Ghosh, 2015) and the number of SD repeats, prolines, and FPR were calculated directly from the sequences.

AUTHOR CONTRIBUTIONS

Alexander Yarawsky: Conceptualization, Methodology, Validation, Formal analysis, Investigation, Writing–Original Draft, Writing–Review & Editing. **Andrea Ori**: Methodology, Formal analysis, Writing–Review & Editing. **Lance English**: Methodology, Formal analysis, Writing–Review & Editing. **Steven Whitten**: Methodology, Formal analysis, Writing–Review & Editing. **Andrew Herr**: Conceptualization, Resources, Writing–Review & Editing, Supervision, Funding acquisition.

ACKNOWLEDGMENTS

Work was performed using funding from NIGMS under R01-GM094363 (to A.B.H.) and R15-GM115603 (to S.T.-W.) and from the University of Cincinnati Graduate School Dean's Fellowship awarded to A.E.Y. (2018-2019 AY). This research used resources of the Advanced Photon Source, a U.S. Department of Energy (DOE) Office of Science User Facility operated for the DOE Office of Science by Argonne National Laboratory under Contract No. DE-AC02-06CH11357. This project was supported by grant P30 GM138395 from the National Institute of General Medical Sciences of the National Institutes of Health. Use of the Pilatus3 X 1M detector was provided by grant 1S10OD018090-01 from NIGMS. The content is solely the responsibility of the authors and does not necessarily reflect the official views of the National Institute of General Medical Sciences of the National Institutes of Health.

CONFLICT OF INTEREST STATEMENT

Andrew B. Herr serves as a Scientific Advisory Board member for Hoth Therapeutics, Inc., holds equity in Hoth Therapeutics and Chelexa BioSciences, LLC, and was a co-inventor on six patents broadly related to the subject matter of this work.

ORCID

Alexander E. Yarawsky https://orcid.org/0000-0002-5973-5058
Andrea L. Ori https://orcid.org/0000-0002-6769-4786
Lance R. English https://orcid.org/0000-0002-1850-7729
Steven T. Whitten https://orcid.org/0000-0003-1364-3956
Andrew B. Herr https://orcid.org/0000-0002-3598-3399

REFERENCES

Adzhubei AA, Sternberg MJ, Makarov AA. Polyproline-II helix in proteins: structure and function. J Mol Biol. 2013;425:2100–32.

Arrecubieta C, Lee MH, Macey A, Foster TJ, Lowy FD. SdrF, a Staphylococcus epidermidis surface protein, binds type I collagen. J Biol Chem. 2007;282:18767–76.

Auton M, Rosgen J, Sinev M, Holthauzen LM, Bolen DW. Osmolyte effects on protein stability and solubility: a balancing act between backbone and side-chains. Biophys Chem. 2011;159: 90–9.

Baskakov I, Bolen DW. Forcing thermodynamically unfolded proteins to fold. J Biol Chem. 1998;273:4831–4.

Baskakov IV, Kumar R, Srinivasan G, Ji YS, Bolen DW, Thompson EB. Trimethylamine N-oxide-induced cooperative folding of an intrinsically unfolded transcription-activating fragment of human glucocorticoid receptor. J Biol Chem. 1999; 274:10693–6.

Bleiziffer I, Eikmeier J, Pohlentz G, McAulay K, Xia G, Hussain M, et al. The plasmin-sensitive protein Pls in methicillin-resistant Staphylococcus aureus (MRSA) is a glycoprotein. PLoS Pathog. 2017;13:e1006110.

Bolen DW, Baskakov IV. The osmophobic effect: natural selection of a thermodynamic force in protein folding. J Mol Biol. 2001; 310:955–63.

Brown PH, Schuck P. Macromolecular size-and-shape distributions by sedimentation velocity analytical ultracentrifugation. Biophys J. 2006;90:4651–61.

Buck M, Schwalbe H, Dobson CM. Characterization of conformational preferences in a partly folded protein by heteronuclear NMR spectroscopy: assignment and secondary structure analysis of hen egg-white lysozyme in trifluoroethanol. Biochemistry. 1995;34:13219–32.

Burchard W. Static and dynamic light scattering approaches to structure determination of biopolymers. In: Harding SE, Satelle DB, Bloomfield VA, editors. Laser Light Scattering in Biochemistry. Cambridge: Royal Society of Chemistry; 1992.

Cantor CR, Schimmel PR. Biophysical chemistry part III: the behaviour of biological macromolecules. New York: W. H. Freeman and Co; 1980.

Cardo D, Horan T, Andrus, M, Dembinski M, Edwards J, Peavy G. National nosocomial infections surveillance (NNIS) system report, data summary from January 1992 through June 2004, issued October 2004. Am. J. Infect. Control. 2004;32:470–485.

Chemes LB, Alonso LG, Noval MG, de Prat-Gay G. Circular dichroism techniques for the analysis of intrinsically disordered proteins and domains. Methods Mol Biol. 2012;895:387–404.

Conrady DG, Brescia CC, Horii K, Weiss AA, Hassett DJ, Herr AB. A zinc-dependent adhesion module is responsible for intercellular adhesion in staphylococcal biofilms. Proc Natl Acad Sci U S A. 2008;105:19456–61.

Corrigan RM, Rigby D, Handley P, Foster TJ. The role of *Staphylococcus aureus* surface protein SasG in adherence and biofilm formation. Microbiology. 2007;153:2435–46.

Creeth JM, Knight CG. On the estimation of the shape of macromolecules from sedimentation and viscosity measurements. Biochimica Biophysica Acta (BBA)–Biophys Includ Photosyn. 1965;102:549–58.

Creighton TE. Proteins: structures and molecular properties. 2nd ed. New York: W.H. Freeman; 1993.

Das RK, Pappu RV. Conformations of intrinsically disordered proteins are influenced by linear sequence distributions of oppositely charged residues. Proc Natl Acad Sci USA. 2013;110:13392–7.

Davis SL, Gurusiddappa S, McCrea KW, Perkins S, Hook M. SdrG, a fibrinogen-binding bacterial adhesin of the microbial surface components recognizing adhesive matrix molecules subfamily from Staphylococcus epidermidis, targets the thrombin cleavage site in the Bbeta chain. J Biol Chem. 2001;276:27799–805.

Drake AF, Siligardi G, Gibbons WA. Reassessment of the electronic circular dichroism criteria for random coil conformations of poly(L-lysine) and the implications for protein folding and denaturation studies. Biophys Chem. 1988;31:143–6.

Dunker AK, Lawson JD, Brown CJ, Williams RM, Romero P, Oh JS, et al. Intrinsically disordered protein. J Mol Graph Model. 2001;19:26–59.

Elam WA, Schrank TP, Campagnolo AJ, Hilser VJ. Evolutionary conservation of the polyproline II conformation surrounding intrinsically disordered phosphorylation sites. Protein Sci. 2013; 22:405–17.

English LR, Tilton EC, Ricard BJ, Whitten ST. Intrinsic alpha helix propensities compact hydrodynamic radii in intrinsically disordered proteins. Proteins. 2017;85:296–311.

English LR, Voss SM, Tilton EC, Paiz EA, So S, Parra GL, et al. Impact of heat on coil hydrodynamic size yields the energetics of denatured state conformational bias. J Phys Chem B. 2019; 123:10014–24.

Fan P, Bracken C, Baum J. Structural characterization of monellin in the alcohol-denatured state by NMR: evidence for beta-sheet to alpha-helix conversion. Biochemistry. 1993;32:1573–82.

Flaugh SL, Lumb KJ. Effects of macromolecular crowding on the intrinsically disordered proteins c-Fos and p27(Kip1). Biomacromolecules. 2001;2:538–40.

Formosa-Dague C, Speziale P, Foster TJ, Geoghegan JA, Dufrene YF. Zinc-dependent mechanical properties of Staphylococcus aureus biofilm-forming surface protein SasG. Proc Natl Acad Sci U S A. 2016;113:410–5.

Foster TJ. Surface proteins of Staphylococcus epidermidis. Front Microbiol. 2020;11:1829.

Foster TJ, Geoghegan JA, Ganesh VK, Hook M. Adhesion, invasion and evasion: the many functions of the surface proteins of Staphylococcus aureus. Nat Rev Microbiol. 2014;12:49–62.

Greenfield NJ. Analysis of circular dichroism data. Methods Enzymol. 2004;383:282–317.

Hazenbos WLW, Kajihara KK, Vandlen R, Morisaki JH, Lehar SM, Kwakkenbos MJ, et al. Novel staphylococcal glycosyltransferases SdgA and SdgB mediate immunogenicity and protection of virulence-associated Cell Wall proteins. PLoS Pathog. 2013;9: e1003653.

Hill CM, Bates IR, White GF, Hallett FR, Harauz G. Effects of the osmolyte trimethylamine-N-oxide on conformation, self-association, and two-dimensional crystallization of myelin basic protein. J Struct Biol. 2002;139:13–26.

Holehouse AS, Das RK, Ahad JN, Richardson MO, Pappu RV. CIDER: resources to analyze sequence-ensemble relationships of intrinsically disordered proteins. Biophys J. 2017;112:16–21.

Hopkins JB, Gillilan RE, Skou S. BioXTAS RAW: improvements to a free open-source program for small-angle X-ray scattering data reduction and analysis. J Appl Cryst. 2017;50:1545–53.

Hussain M, Herrmann M, von Eiff C, Perdreau-Remington F, Peters G. A 140-kilodalton extracellular protein is essential for the accumulation of Staphylococcus epidermidis strains on surfaces. Infect Immun. 1997;65:519–24.

Jarnot P, Ziemska-Legiecka J, Dobson L, Merski M, Mier P, Andrade-Navarro MA, et al. PlaToLoCo: the first web meta-server for visualization and annotation of low complexity regions in proteins. Nucleic Acids Res. 2020;48:W77–84.

Josefsson E, O'Connell D, Foster TJ, Durussel I, Cox JA. The binding of calcium to the B-repeat segment of SdrD, a cell surface protein of Staphylococcus aureus. J Biol Chem. 1998;273: 31145–52.

Kirby N, Cowieson N, Hawley AM, Mudie ST, McGillivray DJ, Kusel M, et al. Improved radiation dose efficiency in solution SAXS using a sheath flow sample environment. Acta Crystallograph Sect D Struct Biol. 2016;72:1254–66.

Konarev PV, Volkov VV, Sokolova AV, Koch MHJ, Svergun DI. PRIMUS: a windows PC-based system for small-angle scattering data analysis. J Appl Cryst. 2003;36:1277–82.

Kumar A, Kumar P, Kumari S, Uversky VN, Giri R. Folding and structural polymorphism of p53 C-terminal domain: one peptide with many conformations. Arch Biochem Biophys. 2020; 684:108342.

Langridge TD, Tarver MJ, Whitten ST. Temperature effects on the hydrodynamic radius of the intrinsically disordered N-terminal region of the p53 protein. Proteins. 2014;82:668–78.

Laue TM, Shah BD, Ridgeway TM, Pelletier SL. Computer-aided interpretation of sedimentation data for proteins. In: Harding SE, Rowe AJ, Horton JC, editors. Analytical ultracentrifugation in biochemistry and polymer science. London: Royal Society of Chemistry; 1992.

Laue TM, Stafford WF 3rd. Modern applications of analytical ultracentrifugation. Annu Rev Biophys Biomol Struct. 1999;28: 75–100.

Lopes JL, Miles AJ, Whitmore L, Wallace BA. Distinct circular dichroism spectroscopic signatures of polyproline II and unordered secondary structures: applications in secondary structure analyses. Protein Sci. 2014;23:1765–72.

Maciag JJ, Chantraine C, Mills KB, Yadav R, Yarawsky AE, Chaton CT, et al. Mechanistic basis of staphylococcal interspecies competition for skin colonization. bioRxiv. 2023.01.26.525635.

Macintosh RL, Brittan JL, Bhattacharya R, Jenkinson HF, Derrick J, Upton M, et al. The terminal a domain of the fibrillar accumulation-associated protein (Aap) of Staphylococcus epidermidis mediates adhesion to human corneocytes. J Bacteriol. 2009;191:7007–16.

Manalastas-Cantos K, Konarev PV, Hajizadeh NR, Kikhney AG, Petoukhov MV, Molodenskiy DS, et al. ATSAS 3.0: expanded functionality and new tools for small-angle scattering data analysis. J Appl Cryst. 2021;54:343–55.

Mao AH, Crick SL, Vitalis A, Chicoine CL, Pappu RV. Net charge per residue modulates conformational ensembles of intrinsically disordered proteins. Proc Natl Acad Sci U S A. 2010;107: 8183–8.

Marsh JA, Forman-Kay JD. Sequence determinants of compaction in intrinsically disordered proteins. Biophys J. 2010;98:2383–90.

Martin EW, Holehouse AS, Grace CR, Hughes A, Pappu RV, Mittag T. Sequence determinants of the conformational properties of an intrinsically disordered protein prior to and upon multisite phosphorylation. J Am Chem Soc. 2016;138:15323–35.

McCrea KW, Hartford O, Davis S, Eidhin DN, Lina G, Speziale P, et al. The serine-aspartate repeat (Sdr) protein family in Staphylococcus epidermidis. Microbiology. 2000;146(Pt 7):1535–46.

McNulty BC, Young GB, Pielak GJ. Macromolecular crowding in the Escherichia coli periplasm maintains alpha-synuclein disorder. J Mol Biol. 2006;355:893–7.

Munishkina LA, Cooper EM, Uversky VN, Fink AL. The effect of macromolecular crowding on protein aggregation and amyloid fibril formation. J Mol Recognit. 2004;17:456–64.

Ntountoumi C, Vlastaridis P, Mossialos D, Stathopoulos C, Iliopoulos I, Promponas V, et al. Low complexity regions in the proteins of prokaryotes perform important functional roles and are highly conserved. Nucleic Acids Res. 2019;47:9998–10009.

Otto M. Staphylococcus epidermidis–the 'accidental' pathogen. Nat Rev Microbiol. 2009;7:555–67.

Pace CN, Trevino S, Prabhakaran E, Scholtz JM. Protein structure, stability and solubility in water and other solvents. Philos Trans R Soc Lond B Biol Sci. 2004;359:1225–34; discussion 1234-1225.

Paharik AE, Kotasinska M, Both A, Hoang TMN, Büttner H, Roy P, et al. The metalloprotease SepA governs processing of accumulation-associated protein and shapes intercellular adhesive surface properties in Staphylococcus epidermidis. Mol Microbiol. 2016;103:860–74.

Perez RB, Tischer A, Auton M, Whitten ST. Alanine and proline content modulate global sensitivity to discrete perturbations in disordered proteins. Proteins. 2014;82:3373–84.

Philo JS. A method for directly fitting the time derivative of sedimentation velocity data and an alternative algorithm for calculating sedimentation coefficient distribution functions. Anal Biochem. 2000;279:151–63.

Philo JS. Improved methods for fitting sedimentation coefficient distributions derived by time-derivative techniques. Anal Biochem. 2006;354:238–46.

Rohde H, Burandt EC, Siemssen N, Frommelt L, Burdelski C, Wurster S, et al. Polysaccharide intercellular adhesin or protein factors in biofilm accumulation of *Staphylococcus epidermidis* and *Staphylococcus aureus* isolated from prosthetic hip and knee joint infections. Biomaterials. 2007;28:1711–20.

Rohde H, Burdelski C, Bartscht K, Hussain M, Buck F, Horstkotte MA, et al. Induction of *Staphylococcus epidermidis* biofilm formation via proteolytic processing of the accumulation-associated protein by staphylococcal and host proteases. Mol Microbiol. 2005;55:1883–95.

Roy P, Horswill AR, Fey PD, Hancock LE, Gilmore MS. Glycan-dependent corneocyte adherence of *Staphylococcus epidermidis* mediated by the lectin subdomain of Aap. MBio. 2021;12: e02908–20.

Rozycka M, Wojtas M, Jakób M, Stigloher C, Grzeszkowiak M, Mazur M, et al. Intrinsically disordered and pliable Starmaker-like protein from medaka (Oryzias latipes) controls the formation of calcium carbonate crystals. PLoS One. 2014;9:e114308.

Rucker AL, Pager CT, Campbell MN, Qualls JE, Creamer TP. Host-guest scale of left-handed polyproline II helix formation. Proteins. 2003;53:68–75.

Sawle L, Ghosh K. A theoretical method to compute sequence dependent configurational properties in charged polymers and proteins. J Chem Phys. 2015;143:085101.

Schaeffer CR, Woods KM, Longo GM, Kiedrowski MR, Paharik AE, Büttner H, et al. Accumulation-associated protein enhances Staphylococcus epidermidis biofilm formation under dynamic conditions and is required for infection in a rat catheter model. Infect Immun. 2015;83:214–26.

Schaub LJ, Campbell JC, Whitten ST. Thermal unfolding of the N-terminal region of p53 monitored by circular dichroism spectroscopy. Protein Sci. 2012;21:1682–8.

Schneewind O, Missiakas D. Sortases, surface proteins, and their raoles in *Staphylococcus aureus* disease and vaccine development. Microbiol Spectrum. 2019;7(1):PSIB-0004-2018.

Sharma N, Fonin AV, Shpironok OG, Silonov SA, Turoverov KK, Uversky VN, et al. Folding perspectives of an intrinsically disordered transactivation domain and its single mutation breaking the folding propensity. Int J Biol Macromol. 2020;155:1359–72.

Shi Z, Chen K, Liu Z, Kallenbach NR. Conformation of the backbone in unfolded proteins. Chem Rev. 2006;106:1877–97.

Shi Z, Chen K, Liu Z, Ng A, Bracken WC, Kallenbach NR. Polyproline II propensities from GGXGG peptides reveal an anticorrelation with beta-sheet scales. Proc Natl Acad Sci U S A. 2005;102:17964–8.

Sonnichsen FD, Van Eyk JE, Hodges RS, Sykes BD. Effect of trifluoroethanol on protein secondary structure: an NMR and CD study using a synthetic Actin peptide. Biochemistry. 1992;31:8790–8.

Speziale P, Pietrocola G, Foster TJ, Geoghegan JA. Protein-based biofilm matrices in staphylococci. Front Cell Infect Microbiol. 2014;4:171.

Stafford WF. Boundary analysis in sedimentation transport experiments: a procedure for obtaining sedimentation coefficient distributions using the time derivative of the concentration profile. Anal Biochem. 1992;203:295–301.

Stetefeld J, McKenna SA, Patel TR. Dynamic light scattering: a practical guide and applications in biomedical sciences. Biophys Rev. 2016;8:409–27.

Tiffany ML, Krimm S. Extended conformations of polypeptides and proteins in urea and guanidine hydrochloride. Biopolymers. 1973;12:575–87.

Tomasso ME, Tarver MJ, Devarajan D, Whitten ST. Hydrodynamic radii of intrinsically disordered proteins determined from experimental Polyproline II propensities. PLoS Comput Biol. 2016;12:e1004686.

Tong SY, Davis JS, Eichenberger E, Holland TL, Fowler VG Jr. Staphylococcus aureus infections: epidemiology, pathophysiology, clinical manifestations, and management. Clin Microbiol Rev. 2015;28:603–61.

Uversky VN. Natively unfolded proteins: a point where biology waits for physics. Protein Sci. 2002a;11:739–56.

Uversky VN. What does it mean to be natively unfolded? Eur J Biochem. 2002b;269:2–12.

Uversky VN. Intrinsically disordered proteins and their environment: effects of strong denaturants, temperature, pH, counter ions, membranes, binding partners, osmolytes, and macromolecular crowding. Protein J. 2009;28:305–25.

Uversky VN, Gillespie JR, Fink AL. Why are "natively unfolded" proteins unstructured under physiologic conditions? Proteins. 2000;41:415–27.

van der Lee R, Buljan M, Lang B, Weatheritt RJ, Daughdrill GW, Dunker AK, et al. Classification of intrinsically disordered regions and proteins. Chem Rev. 2014;114:6589–631.

Whittington SJ, Chellgren BW, Hermann VM, Creamer TP. Urea promotes polyproline II helix formation: implications for protein denatured states. Biochemistry. 2005;44:6269–75.

Yang YH, Jiang YL, Zhang J, Wang L, Bai XH, Zhang SJ, et al. Structural insights into SraP-mediated Staphylococcus aureus adhesion to host cells. PLoS Pathog. 2014b;10:e1004169.

Yarawsky AE, Dinu V, Harding SE, Herr AB. Strong non-ideality effects at low protein concentrations: considerations for elongated proteins. bioRxiv. 2022; 2012.2022.521448.

Yarawsky AE, English LR, Whitten ST, Herr AB. The proline/glycine-rich region of the biofilm adhesion protein Aap forms an extended stalk that resists compaction. J Mol Biol. 2017;429:261–79.

SUPPORTING INFORMATION

Additional supporting information can be found online in the Supporting Information section at the end of this article.

How to cite this article: Yarawsky AE, Ori AL, English LR, Whitten ST, Herr AB. Convergent behavior of extended stalk regions from staphylococcal surface proteins with widely divergent sequence patterns. Protein Science. 2023; 32(8):e4707. https://doi.org/10.1002/pro.4707